



# Prediction of thermal error for feed system of machine tools based on random radial basis function neural network

Tie-jun Li<sup>1</sup> · Ting-ying Sun<sup>1</sup> · Yi-min Zhang<sup>1</sup> · Chun-yu Zhao<sup>2</sup>

Received: 15 July 2020 / Accepted: 11 March 2021 / Published online: 30 March 2021  
© The Author(s), under exclusive licence to Springer-Verlag London Ltd., part of Springer Nature 2021

## Abstract

Thermal errors affect the accuracy of computer numerical control machine tools and are produced by the thermal deformation of machine components due to temperature difference between heat source and ambient temperature of the machine tools. At present, most of the literature does not consider the randomness of the influencing factors of thermal error, leading to inaccurate predictions of machine tool thermal error. In this paper, a new inverse random model is proposed through the combination of the stochastic theory, genetic algorithm, and radial basis function neural network (RBFNN), to predict thermal error while considering the randomness of influencing factors. The randomness index of influencing factors can be identified using the inverse random RBFNN (IR-RBFNN). Furthermore, through the combination of the stochastic theory, RBFNN, and the improved exponential moving average method with abnormal data elimination, a new forward random radial basis function neural network (FR-RBFNN) is established according to the identified influencing factor random index. The models are verified through experimental results on a ball screw system. Compared with the traditional methods, the experimental data show that the proposed method provides a more accurate description of thermal errors while incorporating the randomness of factors affecting thermal error.

**Keywords** Inverse random radial basis function neural network · Genetic algorithm · Prediction model of thermal error · Exponential moving average method · Machine tools

## 1 Introduction

With advances in the manufacturing industry, the demand for machine tools with improved manufacturing accuracy has significantly increased. Recently, the problems associated with the accuracy of machine tools and their solutions have attracted significant attention from researchers. Several studies have shown that thermal and geometric errors are the most critical among various error sources in machine tools. Approximately 40 to 70% of total machine tool errors are caused by thermal deformation [1].

There are two main methods for thermal error prediction. The first method involves calculating the thermal error numerically. The finite element method (FEM) and finite difference method (FDM) are the most commonly used methods for modelling thermal errors. Mian et al. [2] established a thermal error model using the FEM approach. Creighton et al. [3] suggested an FEM model to analyse the temperature field of a milling spindle. Mayr et al. [4] initially proposed an FDM model to calculate the temperature distribution and subsequently developed an FEM model to analyse the thermal error. Zhao et al. [5] used a numerical simulation method to analyse the temperature field and thermal deformation of spindles. Mian et al. [6] applied FEM to simulate the influence of the main internal heat source of a small vertical milling machine. However, the prediction accuracy of thermal errors by FEM and FDM approaches depends on the accurate determination of boundary conditions, such as the heat generation rate and convection heat dissipation. The complex structure and randomness of the machine tool create complex boundary conditions. Most of the existing literature did not consider the randomness of the influencing factors of thermal

✉ Yi-min Zhang  
zhangyimin@syuct.edu.cn

<sup>1</sup> Equipment Reliability Institute, Shenyang University of Chemical Technology, Shenyang 110142, China

<sup>2</sup> School of Mechanical & Automation, Northeastern University, Shenyang 110819, China

errors, which makes it difficult to accurately predict thermal errors.

The second method is to establish the correspondence between system temperatures and thermal errors using artificial intelligence. Various modern intelligent algorithms have been employed to model the thermal errors. Ma et al. [7] used back propagation (BP) and improved BP neural networks to investigate the temperature variables. Li et al. [8] established a modified particle swarm optimisation (PSO) to improve the BP neural network and used it to predict spindle thermal error. Huang et al. [9] used an improved neural network to develop a thermal error prediction method, which improved the convergence speed. Abdulshahed et al. [10] proposed a compensation method for thermal errors in numerically controlled machine tools using the grey neural network model with convolution integral. The PSO algorithm was applied to improve the proposed grey neural network; it simplifies the modelling process and improves the accuracy of the system. Guo et al. [11] presented a new neural network modelling method based on an artificial bee colony and used grey correlation analysis to obtain the system temperature testing points of a machine tool. Similarly, Yang et al. [12] used fuzzy clustering to study the temperature variables. Rojek et al. [13] used the error back propagation, radial basis function neural network, and Kohonen network to study a new ball screw thermal deformation compensation method without sensors. Miao et al. [14] used support vector machines to establish a thermal error model. Cheng et al. [15] proposed a radial basis function (RBF) neural network to calculate the thermal error of a machine tool, which effectively reduced the temperature measurement data points. Wang et al. [16] proposed a method based on clustering thermal sensor data using fuzzy C-means clustering algorithm and iterative self-organising data analysis and established an artificial neural network thermal model. Until now, most of the methods adopted the temperature of the key points collected by the temperature sensor as the input for the intelligent models, which can capture the influence of the heat generation rate and convective heat dissipation. However, the randomness in the measuring error of the temperature sensor itself was not considered in most studies. Moreover, there are chances of abnormal mutation data due to the instability of instrument measurement, which can hinder the accurate prediction of thermal errors.

In summary, most of the literature fails to consider the influence of random factors on thermal errors, which results in poor accuracy of thermal error prediction. To address the above-stated problems, novel inverse random radial basis function neural network (IR-RBFNN) and forward random radial basis function neural network (FR-RBFNN) models are proposed in this paper to accurately predict thermal error while considering the randomness of influencing thermal error factors. First, random input and output variables were introduced into the RBF; subsequently, the genetic algorithm was

selected to obtain the statistical characteristics of the random variables to realise the inverse identification of the random index of influencing factors. Furthermore, the FR-RBFNN was used to predict the thermal error distribution according to the random indices of the identified influencing factors. The experimental results show that the proposed models consider the influence of random factors and can quickly obtain a more accurate description of thermal errors than traditional prediction models.

## 2 Random radial basis function model

The randomness of frictional heat and convection in the feed system causes randomness in the temperature rise. In addition, the randomness of the temperature sensor measurement itself will cause inaccuracies in the thermal error prediction model. Therefore, the randomness of the parameters affecting the thermal errors was considered in the model.

### 2.1 Random temperature field

The randomness of heat generation in friction heat sources, surface convection, and temperature collection measurements causes randomness in the measuring point temperatures.

The temperature field random variables are expressed as follows:

$$T_m = N(\mu_{T_m}, \delta_{T_m}^2) \quad m = 1, 2, \dots, M \quad (1)$$

where  $\mu_{T_m}$ ,  $\delta_{T_m}$ , and  $M$  represent the mean value of the  $m$ th key temperature, standard deviation of the  $m$ th key temperature, and number of temperature key points, respectively.

Considering the influence of random factors on the thermal error, the random variables of the temperature field were used as the inputs.

### 2.2 Random thermal error

The randomness of thermal error was described as follows:

$$e_j = N(\mu_{e_j}, \delta_{e_j}^2) \quad j = 1, 2, \dots, J \quad (2)$$

where  $\mu_{e_j}$ ,  $\delta_{e_j}$ , and  $J$  denote the mean value for the  $j$ th key point thermal error, standard deviation for the  $j$ th key point thermal errors, and number of thermal error key points, respectively.

### 2.3 Random RBFNN model

In this paper, a new random RBFNN model is presented to solve the randomness problem. The structure of the random

RBFNN is illustrated in Fig. 1. The random RBFNN is composed of IR-RBFNN and FR-RBFNN modules.

The radial basis function commonly used in radial basis neural networks is a Gaussian function, and the activation function of the RBFNN can be expressed as follows:

$$H(T_n - d_i) = \exp\left(-\frac{1}{2\sigma^2} \|T_n - d_i\|^2\right) \quad (3)$$

$n = 1, 2, 3, \dots, N \quad i = 1, 2, 3, \dots, I$

where  $T_n = (T_1^n, T_2^n, \dots, T_m^n)^T$  denotes the  $n$ th input sample,  $T$  denotes the temperature vector,  $\|T_n - d_i\|$  denotes the Euclidean norm,  $d_i$  indicates the centre of the  $i$ th node in the hidden layer,  $N$  represents the total number of samples, and  $\sigma$  denotes the variance of the Gaussian function.

However, Eq. 3 was not used to solve the random inputs.

In this study, to solve the random inputs and outputs, Eq. 3 was modified as follows:

$$H(T_n - d_i) = \exp\left(-\frac{1}{2\sigma^2} \|\mu_{Tn} - d_i\|^2\right) \quad (4)$$

$n = 1, 2, 3, \dots, N \quad i = 1, 2, 3, \dots, I$

The output of random RBFNN was further deduced as

$$e_j = \sum_{i=1}^I w_{ij} \exp\left(-\frac{1}{2\sigma^2} \|\mu_{Tn} - d_i\|^2\right) \quad i = 1, 2, 3, \dots, I \quad j = 1, 2, 3, \dots, J \quad (5)$$

where  $w_{ij}$  denotes the connection weight of the  $i$ th node of the hidden layer to the  $j$ th node of the output layer,  $I$  represents the number of hidden layer nodes, and  $e_j$  denotes the output value of the  $j$ th output node.

The variance  $\sigma_i$  of random RBFNN was expressed as follows:

$$\sigma_i = \frac{D_{\max}}{\sqrt{2I}} \quad (i = 1, 2, \dots, I) \quad (6)$$

where  $D_{\max}$  denotes the maximum distance between centres. The least-squares method was used to calculate the connection weights from the hidden layer to the output layer.

In this study, the connection weights between the hidden and output layers are obtained as shown in Eq. 7.

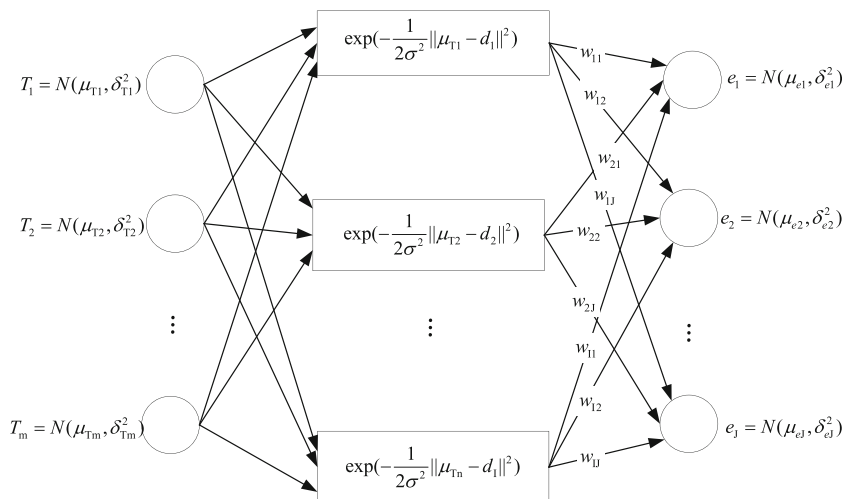
$$w = \exp\left(-\frac{I}{D_{\max}^2} \|\mu_{Tn} - d_i\|^2\right) \quad i = 1, 2, \dots, I \quad n = 1, 2, \dots, N \quad (7)$$

### 2.3.1 IR-RBFNN model

To accurately investigate the randomness of the parameters in practical applications, the standard deviation in the input of the key point temperatures was obtained from inverse identification through the experiments. Hence, a genetic algorithm (GA), which is a parallel stochastic search optimisation method, was combined with a random RBFNN to realise inverse random parameter identification.

In this study, the generated random variables were used as the input of the trained random RBFNN. Initially, the simulation calculation was repeated  $K$  times. From the results of the  $K$  times simulations, the mean value and standard deviation of the random parameters were obtained. Then, the mean value differences and the standard deviation between the simulation results and experimental data were used as the individual fitness values to execute GA. Subsequently, random RBFNN and GA were combined. The differences in the mean values and the standard deviation between the simulation results and experimental data were the objective functions, and the minimum values of the two objective functions were searched by GA.

Fig. 1 Structure of random RBFNN



**Encode** In this study, individual coding was real number coding. During the execution of the genetic algorithm, the initial variables  $T$  and  $\delta$  were coded separately.

**Fitness function** The absolute value of the mean difference between the simulated results and the experimental data was used for the individual fitness value  $F_1$ , which can be expressed as

$$F_1 = \text{abs}(\mu_e^{\text{Sim}} - \mu_e^{\text{Exp}}) \quad (8)$$

where  $\mu_e^{\text{Exp}}$  represents the mean value of the measuring results obtained through experiment.

The mean value of the thermal errors  $\mu_e^{\text{Sim}}$  of the random RBFNN simulation output is expressed as

$$\mu_e^{\text{Sim}} = \frac{\sum_{k=1}^K \mu_{ej}^k}{K} \quad (9)$$

where  $K$  represents the number of repeated simulations with random parameters and  $\mu_{ej}^k$  denotes the mean value of the  $j$ th key point thermal error after simulations repeated  $k$ .

The absolute value of the standard deviation difference between the simulation calculation and the experimental data was used for the individual fitness value  $F_2$ , which can be expressed as

$$F_2 = \text{abs}(\delta_e^{\text{Sim}} - \delta_e^{\text{Exp}}) \quad (10)$$

where  $\delta_e^{\text{Exp}}$  denotes the standard deviation of the measuring data.

The standard deviation  $\delta_e^{\text{Sim}}$  of the network simulation output value is expressed as

$$\delta_e^{\text{Sim}} = \sqrt{\frac{\sum_{k=1}^K (\mu_{ej}^k - \mu_e^{\text{Sim}})^2}{K}} \quad (11)$$

**Selection, crossover, and mutation operations** The selection operation in GA directly affects its performance. In this algorithm, the probability of its selection  $p_i$  was obtained as follows:

$$p_i = \frac{f_i}{\sum_j^N f_j} \quad (12)$$

where  $f_i = 1/F_i$ .  $F_i$  indicates the fitness value of the individual  $X_i$ , and  $N$  denotes the number of population individuals.

The real crossover method was used in this study, and the  $g$  chromosome  $z_g$  and the  $h$  chromosome  $z_h$  are used in the  $l$  bit cross operation method as follows:

$$\left. \begin{aligned} z_{gl} &= z_{gl}(1-r) + z_{hl}r \\ z_{hl} &= z_{hl}(1-r) + z_{gl}r \end{aligned} \right\} \quad (13)$$

where  $r$  represents a random number between  $[0, 1]$ .

### 2.3.2 FR-RBFNN model

To predict the thermal errors accurately while considering the randomness of the parameters, random inputs  $T_m = N(\mu_{Tm}, \delta_{Tm}^2)$  were introduced to the RBFNN. The standard deviation  $\delta_{Tm}$  of the inputs was obtained from the identification of the IR-RBFNN.

In most of the existing literature, the inputs of the network are obtained directly by reading temperature data from the sensors. Although this method can obtain the key point temperature data, this data contains the randomness of the instrument's measurement. Furthermore, large amounts of abnormal data caused by instrument instability may occur. Directly reading the data cannot exclude the measurement error of the instrument, which affects the accuracy of the thermal error prediction.

In this paper, a new real-time dynamic moving average algorithm is proposed to solve the problem of randomness and instability caused by instrument measurement errors.

The exponential moving average algorithm can be written as

$$F_{i+1} = \alpha Y_t + (1-\alpha)\alpha Y_{t-1} + (1-\alpha)^2 \alpha Y_{t-2} + \dots + (1-\alpha)^n \alpha Y_{t-n} + \dots + (1-\alpha)^t F_i \quad (14)$$

where  $Y_t$ ,  $\alpha$ ,  $F_t$ , and  $F_{i+1}$  represent the actual measuring value of the  $t$ th period, smoothing coefficient, average prediction value of the  $t$ th period, and average prediction value of the  $(t+1)$ th period, respectively.

Equation 14 is suitable for data without abnormal mutation. However, owing to the instability of instrument measurements, there is a probability of abnormal mutation data occurrence. Therefore, this method is not applicable in our case.

In this paper, an improved real-time dynamic moving average algorithm that eliminates abnormal mutation data is proposed.

The mutation value was identified by comparing the predicted and measured values. If the difference between the predicted and measured values is larger than the mutation threshold, the measured value considered abnormal and will be replaced by the predicted value.

$$\left. \begin{aligned} |Y_{t+1} - F_{i+1}| &> \Delta, Y_{t+1} = F_{i+1} \\ |Y_{t+1} - F_{i+1}| &< \Delta, Y_{t+1} = Y_{t+1} \end{aligned} \right\} \quad (15)$$

where  $\Delta$  represents the mutation threshold.

This method is suitable for removing abnormal mutations in gradually changing signals; the temperature rise in machine tools corresponds to gradually changing signals.

Using the real-time measuring temperature data, the mean  $\mu_{Tm}$  of the inputs can be obtained through the new real-time dynamic moving average algorithm.

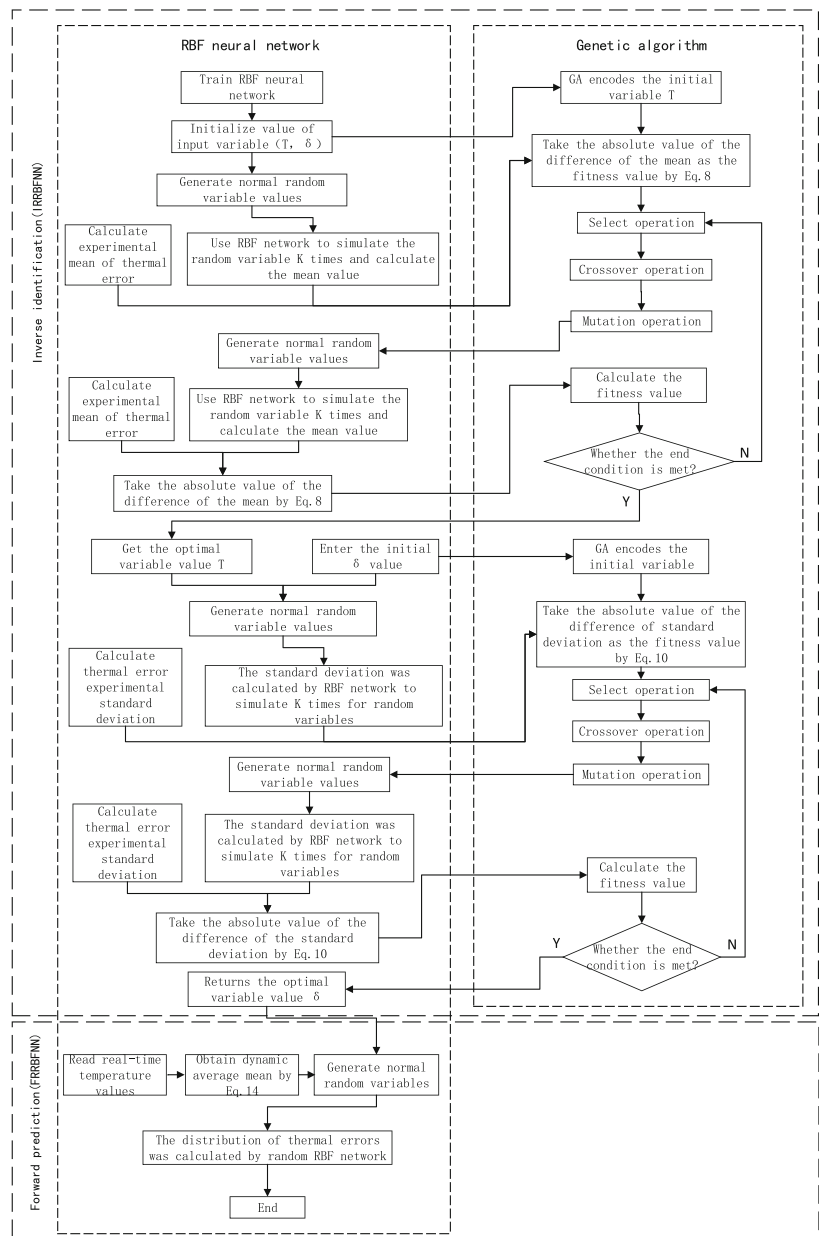
### 2.4 Flowchart of the random RBF model

The algorithm consists of IR-RBFNN and FR-RBFNN modules. The IR-RBFNN module realises random parameter identification, and the FR-RBFNN module completes the thermal error prediction. A flowchart for random RBFNN is shown in Fig. 2.

In this study, an IR-RBFNN model was first established, which uses GA for searching the dataset to obtain the distribution characteristics of random parameters. Subsequently, the FR-RBFNN model was used for thermal error prediction. The implementation process is as follows:

- 1) The RBFNN was trained with experimental data to obtain the network model.
- 2) The  $\mu_{Tm}$  and  $\sigma_{Tm}$  values of the initial variables were set, and the *normrnd* function was used to generate the values of normal random variable, which were used as an IR-RBFNN input. The mean of the thermal error  $\mu_e^s$  was obtained as output after the network repeated the

Fig. 2 Algorithm flowchart of the random RBFNN





- simulation  $Q$  times. The difference between the mean of the random RBF output and the mean of the experimental thermal error was calculated.
- 3) The GA was first used to encode the initial temperature variable, and the absolute difference of the mean value was considered the fitness value. Subsequently, selection, crossover, and mutation were performed to generate a normal random variable for each new individual, and the network simulation was iterated  $K$  times to produce the output.
  - 4) The fitness value  $F_1$  was calculated through Eq. 8. If the fitness value did not meet the conditions, the model returned to the selection operation and repeated the cycle until the best fitness value was obtained. If the required conditions were met, the results were directly considered output. Finally, the optimal value of the temperature variable was returned, and the inverse identification of the mean of the temperature input was realised.
  - 5) The initial temperature variable was updated by replacing the original temperature with the optimal temperature. Then, *normrnd* function was used to generate the normal random variable values, RBFNN was used again, and thermal error standard deviation  $\delta_e^s$  was obtained after  $Q$  iterations. The difference between the standard deviation of the output thermal error and the measured thermal error was determined.
  - 6) The GA was used to encode the standard deviation of the initial temperature. The absolute value of the difference in the standard deviation was considered the fitness value according to Eq. 10, and the selection, crossover, and mutation were carried out. The new individuals obtained were generated into the normal random variables again, and the network simulation was continued  $K$  times to output the thermal error standard deviation. Then, the operation of fitness value was calculated. If the fitness value did not meet the conditions, the model returned to the selection operation and repeated the cycle until the best fitness value was obtained. If the required conditions were met, the results were considered output directly. Finally, the optimal temperature standard deviation was returned; that is, the reverse identification of the temperature standard deviation was realised.
  - 7) Using the real-time temperature value read from the sensors, the mean  $\mu_{T_m}$  of the inputs can be obtained by the new real-time dynamic moving average algorithm.
  - 8) According to the results of step 7, the random variables were generated and then used in the FR-RBFNN to complete the thermal error prediction.

### 3 Experimental setup and testing process

#### 3.1 Experimental setup

In this study, the thermally deduced positioning error of a ball screw system was investigated experimentally using a computer numerical control (CNC) lathe. The entire experimental device was composed of a CNC lathe, laser interferometer, temperature acquisition equipment, and microcomputers, as shown in Fig. 3.

A random time-varying prediction model based on an  $x$ -axis feed system is investigated in this study. Table 1 lists the parameters of the system.

#### 3.2 Distribution of measuring points

The three temperature measuring points  $T_1$ ,  $T_2$ , and  $T_3$  were at the bearing 1 seat, screw-nut flange, and bearing 2 seat, respectively. The stroke of the thermal error measuring points was 220 mm, and 6 measuring points P1–P6 were evenly distributed, as shown in Fig. 4.

**Fig. 3** Components of experimental device

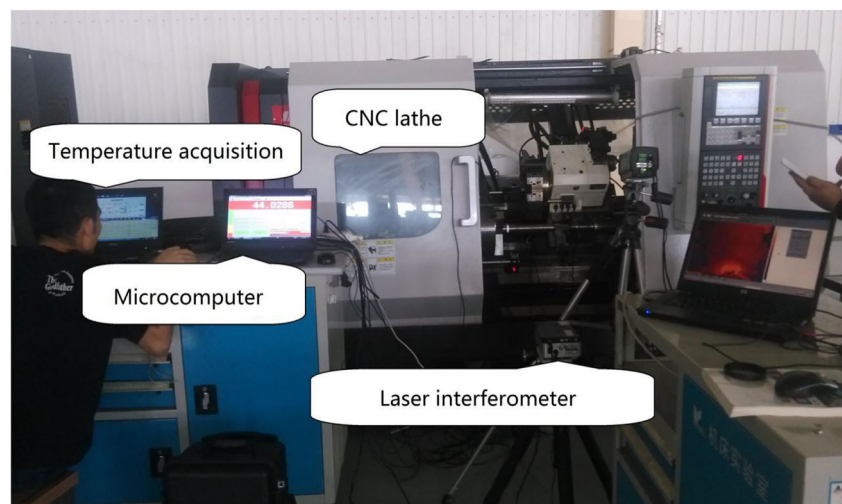


**Table 1** Parameters of the *x*-axis system

Parameters	Symbols	Value (mm)
Screw length	$L_s$	300
Screw diameter	$d$	32
Screw lead	$p$	10
Screw Stroke	$L$	220
Inner diameter of the bearings	$D_i$	30
Outer diameter of the bearings	$D_o$	62
Width of the bearings	$B$	16

According to ISO 230–2 standards, the temperature of key points  $T_1$ ,  $T_2$ , and  $T_3$  were observed by a thermocouple at an interval of 0.5 s. The positioning error of the system was recorded using a laser interferometer. The positioning errors of uniformly distributed P1–P6 points were recorded at a distance of 44 mm between the measuring points. During the experimental measurement, the lathe was operated at a feed rate of 15 m/min. Positioning errors of points P1–P6 after heating on the lathe for 10, 20, 30, 40, and 50 min were measured and recorded with a laser interferometer. In this study, 30 independent experiments were conducted under the same initial and operating conditions. Under a constant temperature without a cutting load, the thermal error caused by screw rotation at a spindle speed of 0 r/min was measured. The time-varying random prediction model of the random RBFNN was verified through 30 cutting-free load tests.

### 4 Results and discussion

In this study, the measured values of the three temperature sensors and the corresponding thermal errors of the measuring points were considered the training data set. A set of temperature and thermal error values were recorded after every 10 min, and 30 sets of data were selected as training sets to train the RBFNN. The *normrnd* function was used to generate the normal random temperature variables as input to predict the thermal errors. The mean and standard deviation of the

thermal error were calculated using the random RBFNN and compared with those obtained from the experimental data.

The standard deviation of the thermal error was calculated from the experimental data, and the value was  $\delta_e = 0.029$ . The parameters of GA used in this study are listed in Table 2.

Figures 5, 6, and 7 show the axial thermal errors of the screw obtained by the random RBFNN model, FEM simulation, and experiment for heating the machine under a feed rate of 15 m/min for 10, 30, and 50 min, respectively. As shown from these figures, the mean value of the thermal error calculated by the random RBFNN is in good agreement with the mean value of the experimental values and FEM calculation results. The upper and lower limits of the thermal error calculated by the random RBFNN are in good agreement with the experimental data of the system. Moreover, the standard deviation of the thermal error is in good agreement with the experimental data.

In addition, there are some differences between the random RBFNN model and the FEM simulation results.

Figure 5 shows the thermal error distribution at different screw positions at the 10th min. According to the FEM results, the screw thermal error from 0 to 176 mm is less than the threshold value of 10  $\mu\text{m}$ , which is deemed “qualified.” However, according to the random RBFNN model and experimental data, the failure probability of the screw gradually increased from 0 to 50%—from 150 to 176 mm. According to the FEM results, when the thermal error of the screw from 176 to 220 mm is larger than the threshold value of 10  $\mu\text{m}$ , this is considered “failure.” However, according to the random RBFNN model and experimental data, the screw failure probability from 176 to 215 mm gradually increased from 50 to 100%.

Figure 6 shows the thermal error at different positions of the screw at 30th min. Based on the FEM results, when the thermal error of the screw from 0 to 110 mm is less than the threshold value of 10  $\mu\text{m}$ , it is considered “qualified,” similar to the 10th min case. However, according to the random RBF model and the measured data, the failure probability of the screw from 100 to 110 mm gradually increased from 0 to 50%. According to the FEM results, when the thermal error of the screw from 110 to 220 mm is larger than the threshold value of 10  $\mu\text{m}$ , it is considered “failure.” However, according

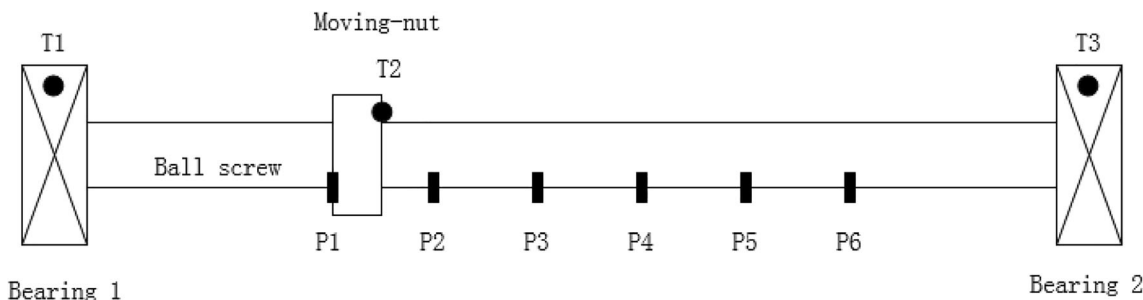


**Fig. 4** Structure of feed system and distribution of measurement points

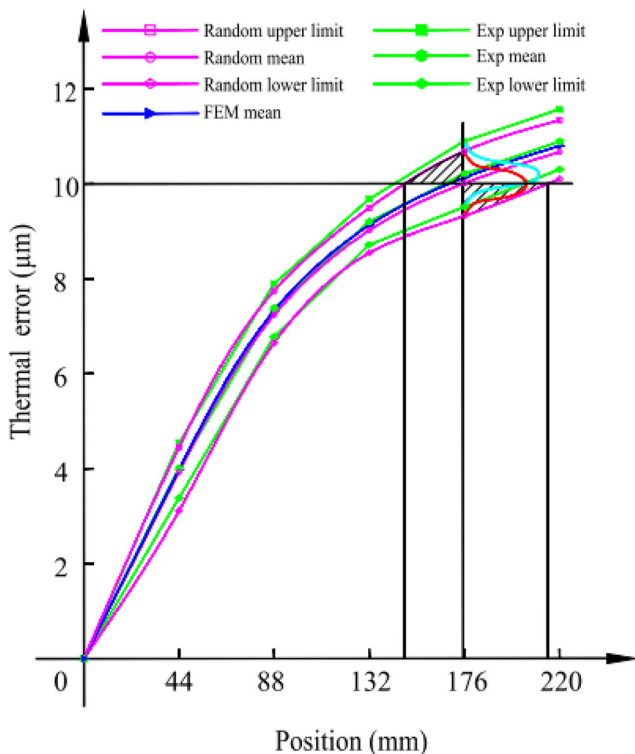
**Table 2** The parameters of GA

Parameters	Symbols	Value
Population size	$S$	20
Number of evolution	$G$	5
Crossover probability	$P_C$	0.4
Mutation probability	$P_M$	0.2

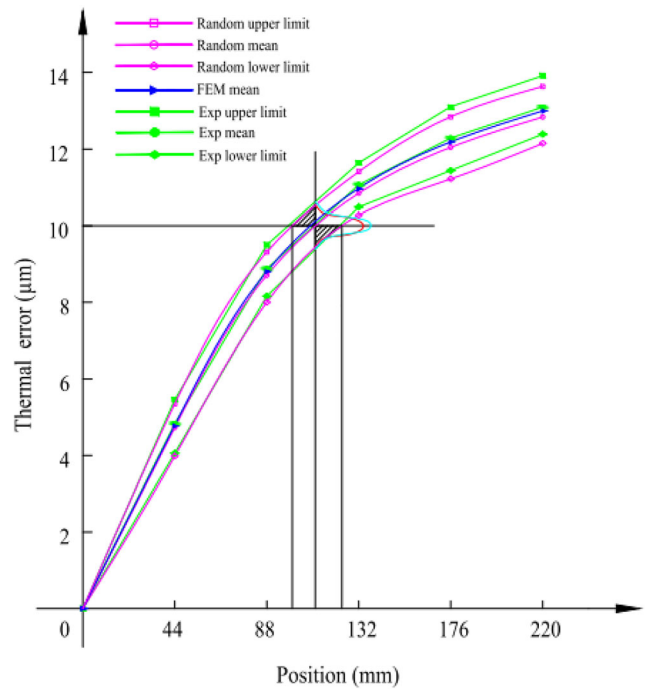
to the random RBFNN model and experimental data, the failure probability from 110 to 123 mm gradually increased from 50 to 100%.

Figure 7 shows the thermal error at different positions of the screw at 50th min. Based on the FEM simulation, the screw thermal error from 0 to 98 mm is less than the threshold value of 10  $\mu\text{m}$ , which is deemed qualified, similar to the 10th min case. However, according to the random RBFNN model and the measurement results, the failure probability of the screw from 87 to 98 mm gradually increases from 0 to 50%. The FEM simulation results indicate that the thermal error of the screw from 98 to 220 mm is larger than the threshold value of 10  $\mu\text{m}$ , which denotes failure. However, according to the random RBFNN model and experimental data, the failure probability from 98 to 110 mm gradually increases from 50 to 100%.

From Figs. 5, 6, and 7, it can be seen that the random RBF model proposed herein considers the parameter randomness.



**Fig. 5** Thermal error at different positions of screw at the 10th min



**Fig. 6** Thermal error at different positions of screw at the 30th min

Hence, it can describe the real-time thermal error of the screw from the perspective of reliability, which is more accurate.

In addition, the aforementioned results show that the mean value and the discreteness of the thermally induced error of the screw were affected by the mean value and standard deviation of the random variable. In this study, because the influence of random factors is considered, the prediction results of the random RBFNN model are more accurate than those of the FEM.

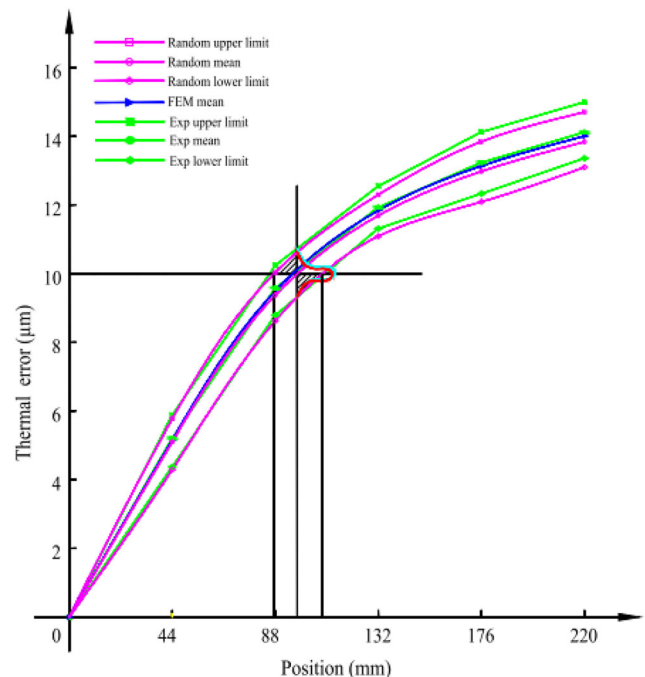


**Fig. 7** Thermal error at different positions of screw at the 50th min



Moreover, the running time of the random RBFNN prediction model was approximately 190 ms and that of the FEM model was approximately 50 min. The comparison results show that the running speed of the proposed model is significantly higher than that of the FEM model. Therefore, the random RBFNN prediction model can quickly obtain accurate results.

## 5 Conclusions

In this study, a novel IR-RBFNN model is proposed by combining the stochastic theory, GA, and RBFNN. Subsequently, using IR-RBFNN, the randomness index of the influencing factors was identified. Furthermore, through the combination of the stochastic theory, RBFNN, and the modified exponential moving average method with abnormal data elimination, the FR-RBFNN model is established according to the identified influencing factor random index. Using the two models, a novel prediction model for thermal error is proposed, considering the randomness of factors affecting the thermal error. This work considers the randomness of the friction heat, ambient temperature, and equipment measurement that directly affect the accuracy of thermal error prediction of the feed system. Compared with the traditional method, the experimental data of the lathe show that the proposed random RBFNN can obtain a more accurate error description considering the randomness of factors affecting thermal error.

**Author contribution** Tie-jun Li: conceptualization, methodology. Ting-ying Sun: software, writing - original draft preparation. Yi-min Zhang: supervision. Chun-yu Zhao: validation.

**Funding** This work was supported by the project from the Department of Education of Liaoning Province [No. LJ2020031]. Simultaneously it was supported by the National Natural Science Foundation of China under [Grants U1708254].

**Availability of data and material** The data cannot be shared openly, to protect study participant privacy.

**Code availability** The code cannot be shared openly, to protect study participant privacy.

## Declarations

**Conflict of interest** The authors declare no competing interests.

## References

- Bryan J (1990) International status of thermal error research (1990). *CRIP Annals Manuf Technol* 39:645–656. [https://doi.org/10.1016/S0007-8506\(07\)63001-7](https://doi.org/10.1016/S0007-8506(07)63001-7)
- Mian NS, Fletcher S, Longstaff AP, Myers A (2013) Efficient estimation by FEA of machine tool distortion due to environmental temperature perturbations. *Precis Eng* 37:372–379. <https://doi.org/10.1016/j.precisioneng.2012.10.006>
- Creighton E, Honegger A, Tulsian A, Mukhopadhyay D (2010) Analysis of thermal errors in a high-speed micro-milling spindle. *Int J Mach Tools Manuf* 50:386–393. <https://doi.org/10.1016/j.ijmachtools.2009.11.002>
- Mayr J, Ess M, Weikert S, Wegener K (2009) Compensation of thermal effects on machine tools using a FDEM simulation approach Proceedings of the 9th LAMDAMAP, pp 38–47
- Haitao Z, Jianguo Y, Jinhua S (2007) Simulation of thermal behavior of a CNC machine tool spindle. *Int J Mach Tools Manuf* 47:1003–1010. <https://doi.org/10.1016/j.ijmachtools.2006.06.018>
- Mian NS, Fletcher S, Longstaff AP, Myers A (2011) Efficient thermal error prediction in a machine tool using finite element analysis. *Meas Sci Technol* 22:085107. <https://doi.org/10.1088/0957-0233/22/8/085107>
- Ma C, Zhao L, Mei XS, Shi H, Yang J (2017) Thermal error compensation of high-speed spindle system based on a modified BP neural network. *Int J Adv Manuf Technol* 89:3071–3085. <https://doi.org/10.1007/s00170-016-9254-4>
- Li B, Tian XT, Zhang M (2019) Thermal error modeling of machine tool spindle based on the improved algorithm optimized BP neural network. *Int J Adv Manuf Technol* 105:1497–1505. <https://doi.org/10.1007/s00170-019-04375-w>
- Huang YQ, Zhang J, Li X, Tian LJ (2014) Thermal error modeling by integrating GA and BP algorithms for the high-speed spindle. *Int J Adv Manuf Technol* 71:1669–1675. <https://doi.org/10.1007/s00170-014-5606-0>
- Abdulshahed AM, Longstaff AP, Fletcher S, Potdar A (2016) Thermal error modelling of a gantry-type 5-axis machine tool using a Grey Neural Network Model. *J Manuf Syst* 41:130–142. <https://doi.org/10.1016/j.jmsy.2016.08.006>
- Guo QJ, Fan S, Xu RF, Cheng X, Zhao GY, Yang JG (2017) Spindle thermal error optimization modeling of a five-axis machine tool. *Chin J Mech Eng* 30:746–753. <https://doi.org/10.1007/s10033-017-0098-0>
- Yang J, Shi H, Feng B, Zhao L, Ma C, Mei XS (2015) Thermal error modeling and compensation for a high-speed motorized spindle. *Int J Adv Manuf Technol* 77:1005–1017. <https://doi.org/10.1007/s00170-014-6535-7>
- Rojek I, Kowal M, Stoic A (2017) Predictive compensation of thermal deformations of ball screws in CNC machines using neural networks. *Tehn Vjesn* 24:1697–1703. <https://doi.org/10.17559/TV-20161207171012>
- Miao EM, Gong YY, Niu PC, Ji CZ, Chen HD (2013) Robustness of thermal error compensation modeling models of CNC machine tools. *Int J Adv Manuf Technol* 69:2593–2603. <https://doi.org/10.1007/s00170-013-5229-x>
- Cheng Q, Qi Z, Zhang G, Zhao Y, Sun B, Gu P (2016) Robust modelling and prediction of thermally induced positional error based on grey rough set theory and neural networks. *Int J Adv Manuf Technol* 83:753–764. <https://doi.org/10.1007/s00170-015-7556-6>
- Wang HT, Wang LP, Li TM, Han J (2013) Thermal sensor selection for the thermal error modeling of machine tool based on the fuzzy clustering method. *Int J Adv Manuf Technol* 69:121–126. <https://doi.org/10.1007/s00170-013-4998-6>

**Publisher's note** Springer Nature remains neutral with regard to jurisdictional claims in published maps and institutional affiliations.